Aggregates Dramatically Alter Fibrin Ultrastructure

Xabel García, Landry Seyve, Zera Tellier, Guillaume Chevreux, Nicolas Bihoreau, Benoît Polack, Francois Caton

▶ **To cite this version:**

Xabel García, Landry Seyve, Zera Tellier, Guillaume Chevreux, Nicolas Bihoreau, et al.. Aggregates Dramatically Alter Fibrin Ultrastructure. Biophysical Journal, 2020, 118, pp.172 - 181. 10.1016/j.bpj.2019.10.034 . hal-03489348

HAL Id: hal-03489348
https://hal.science/hal-03489348v1

Submitted on 7 Mar 2022

HAL is a multi-disciplinary open access archive for the deposit and dissemination of scientific research documents, whether they are published or not. The documents may come from teaching and research institutions in France or abroad, or from public or private research centers.

L'archive ouverte pluridisciplinaire **HAL**, est destinée au dépôt et à la diffusion de documents scientifiques de niveau recherche, publiés ou non, émanant des établissements d'enseignement et de recherche français ou étrangers, des laboratoires publics ou privés.

Distributed under a Creative Commons Attribution - NonCommercial 4.0 International License

Version of Record: https://www.sciencedirect.com/science/article/pii/S0006349519308963
Manuscript_16c672ecb50ae6989e298db06a80a3d0

Aggregates dramatically alter fibrin ultrastructure

Authors:

Xabel GARCÍA[1], Landry SEYVE[2,3], Zera TELLIER[4], Guillaume CHEVREUX[4], Nicolas BIHOREAU[4], Benoît POLACK[2,3], and Francois CATON[1]

1 Université Grenoble Alpes, Laboratoire Rhéologie et Procédés, UMR CNRS 5520= , Grenoble, France
2 Université Grenoble Alpes, TIMC-TheREx, UMR CNRS 5525, Grenoble, France
3 Centre Hospitalier Universitaire Grenoble Alpes, Département d'Hématologie, Institut de Biologie et de Pathologie, Grenoble, France
4 Laboratoire Français du Fractionnement et des Biotechnologies, 3 Avenue des Tropiques, 91958 Courtaboeuf (Les Ulis), France

© 2019 published by Elsevier. This manuscript is made available under the CC BY NC user license
https://creativecommons.org/licenses/by-nc/4.0/

Abstract

Among the many factors influencing fibrin formation and structure (concentration, temperature, composition, pH…), it has been suggested that the polydispersity of fibrinogen may play an important role. We propose here a detailed investigation of the influence of this parameter on fibrin multiscale structure.

Two commercial fibrinogen preparations were used, a monodisperse and a polydisperse one. First, the respective compositions of both fibrinogen preparations were thoroughly determined by measuring the FXIII, fibronectin, α, β and γ intact-chains contents, the γ/γ′ chains ratio, the N-glycosylation and the post-translational modifications. Slight variations between the composition of the two fibrinogen preparations were found which are much smaller than the compositional variations necessary to alter significantly fibrin multiscale structure as observed in the literature. Conversely, MALLS coupled SEC and DLS measurements showed that the polydisperse preparation contains significant amounts of aggregates while the other preparation is essentially monodisperse.

The multiscale structure of the fibrins produced from those two fibrinogen preparations was determined by using X-ray scattering, spectrophotometry, and confocal microscopy. Results show that fibers made from the aggregate-free fibrinogen present a crystalline longitudinal and lateral structure and form a mikado-like network. The network produced from the aggregates-containing fibrinogen looks to be partly build around bright spots which are attributed to the aggregate. The multiscale structure of mixtures between the two preparations shows a smooth evolution, demonstrating that the quantity of aggregates is a major determining factor for fibrin multiscale structure. Indeed, the effect of a few percent in mass of aggregates is larger than any other effect due to compositional differences under the same reaction conditions. Finally we propose a mechanistic interpretation of our results which points at a direct role of the aggregates during polymerization which disrupt the ideal ordering of monomers inside fibrin protofibrils and fibers.

Statement of Significance

Fibrin formation, structure and properties are major biophysical topics because of their potential relevance to cardiovascular and thrombo-embolic diseases. While there has been a recent surge of work in this area, most studies used the same fibrinogen provider and therefore possessed very similar compositional and polydispersity profiles. We show that different fibrinogen preparations with identical compositions but containing or not fibrinogen aggregates

produce fibrins with different structures, uncovering a new and essential control parameter. Results strongly suggest that characterization by size exclusion chromatography should be systematically performed to ensure that results are comparable from study to study. Furthermore, the importance of the modifications due to relatively minute amounts of aggregates suggests that they may play a major role in fibrin polymerization.

1 Introduction

The formation of the fibrin clot is essential in the process of blood coagulation. Fibrin forms a protein scaffold that enables the organism to close off damaged blood vessels. In the first step of fibrin formation, the fibrinopeptides A and B from the protein fibrinogen are cleaved by thrombin, producing the so-called fibrin monomers which then polymerize into a fibrin network. Fibrinogen itself is a plasma 340-kDa centrosymetric protein. Its structure is constituted by three aligned domains. The central part of the molecule (E-region) is slightly smaller (c.a. 5nm of diameter) while the distal regions (D-regions) present a 6nm diameter to form a structure about 45nm in length.

While some aspects of the formation of the fibrin network from fibrin monomers are still under debate, it is known that various genetic and environmental factors influence not only the fibrin structure and function but that they can also be related with thrombotic disease (e.g. 1). Indeed, many clinical studies have associated the fibrin properties with thrombosis (2, 3). Among the many factors influencing fibrin polymerization, structure and function (ionic strength, pH, concentrations, γ' content … (4-10)), Huang et al. (11,12) suggested that the size dispersity, i.e. the amount of aggregates or oligomers present in the fibrinogen preparation, may play an important role. Indeed, fibrins made from chromatography fractionated fibrinogen exhibited final turbidities between two and three times higher than the unfractionated samples (11), and significant differences both in kinetics as well as in the apparent size of the polymerizing objects were observed in a later study (12). However, a Small Angle X-Ray Scattering study of this fractionation process showed significant in–column degradation (13) and gel filtration could change the concentration in important proteins present in the fibrinogen preparations (called co-purified proteins), such as fibronectin, FXIII, … Likewise, fibrinogen isoforms (γ' content, oxidized forms, N-/C-terminus cleaved forms, …) may be prone to variability during the chromatography fractionation process and therefore to behave specifically *vis-à-vis* polymerization.

As the relative compositions of the mono- and poly-disperse fibrinogen preparations were not characterized nor the molar masses of the different fractions measured, the question of whether the observed effect is a consequence of variations in aggregate content and/or composition remains open. Furthermore, single-wavelength optical-density measurements only indicate an overall change in fibrin structure but provide no indication about the morphological changes or the scale(s) affected, nor about the involved mechanisms.

In the last decade or so, about 2/3rd of the fundamental work on fibrin formation has been performed on fibrinogen from Enzyme Research Laboratories (see Supporting Information (SI.1), hence with rather constant compositional and polydispersity profiles. While this is pertinent for comparison purposes, the effect of fibrinogen's polydispersity was mostly overlooked in the current fibrin-related literature, while it is a well-known factor in standard polymer science (e.g. 14).

The above observations raise four important questions. First, does fibrinogen dispersity really influence the multiscale structure of fibrin, or were Huang et al. observations (11) a consequence of the purification procedure they used? Second, what are the scales affected by dispersity and how are those scales affected? Third, are those differences also observed at physiological fibrinogen concentrations (2-4 mg/ml) or limited to the very low concentrations used in previous studies? Finally, are the dispersity-induced structural effects important? In other words, are they smaller or larger than those induced by varying compositional aspects of the fibrinogen preparations?

In the following, we start by describing the numerous experimental methods used in this work. To characterize the two fibrinogens, we performed Refractive index and MALLS-coupled Size Exclusion Chromatography, Dynamic Light Scattering, Reverse phase chromatography coupled to mass spectrometry, and all necessary co-purified proteins quantification assays. The methods used to determine the structure of the fibrins at each scale are then described, starting with Small Angle X-Ray Scattering, Spectrophotometry, and finally Confocal Microscopy.

Then, we present the detailed characterization of the physical and physicochemical properties of the different fibrinogens, showing that the two fibrinogens used in this study present identical compositional profiles while differing only in their aggregate content. We then investigate the effect of this size dispersity on the nano- and micro-scale structure of the fibrin, showing that the two fibrins present vastly different structures, at all scales. We finally discuss the present findings in the light of recent results concerning the effect of compositional and isoform changes on fibrin structure and propose a mechanistic explanation of our results.

2 Materials and Methods

Materials

Human thrombin was purchased from Cryopep (Montpellier, France) as a 12 µL solution containing 298,9 IU. The solution was diluted to 200 IU/ml in a 2-(N-morpholino)ethanesulfonic (MES) buffer (20mM MES, 50mM NaCl, pH 6.5) aliquoted and kept frozen at -80°C.

Two fibrinogens were used: Clottafact (Laboratoire Français du Fractionnement et des Biotechnologies, Les Ulis, France) and Fib1 (Enzyme Research Laboratories, Swansea, UK). In the following, Clottafact will be termed as FibWoA for Fibrinogen WithOut aggregates, while Fib1 will be termed as FibWA for Fibrinogen With aggregates. The reason for this terminology will be become apparent in the SEC and DLS results.

Fibrinogens were reconstituted using manufacturers' guidelines: Fib1 and Clottafact fibrinogens were reconstituted by adding respectively 25 mL and 100 mL of Sterile Water for Injection into the product vials. Then, the product vials were incubated at 37° C and gently swirled until the product was fully dissolved. Both fibrinogens were dialyzed together twice overnight against >100 volumes of HEPES buffer (140 mM NaCl, 20 mM HEPES, 5 mM $CaCl_2$, pH 7.4), aliquoted and kept frozen at -80° C. Fibrinogen concentrations were determined by absorbance at 280 nm using a specific absorption coefficient of E^{280}= 1.51 ml·mg^{-1}·cm^{-1}.

Dithiothreitol (DTT), iodoacetamide (IAM), urea, phosphate buffered saline (PBS), ammonium carbonate, and HEPES were purchased from Sigma-Aldrich Chemical (St. Louis, MO, USA). Acetonitrile (MeCN) was HPLC reagent grade and purchased from JT Baker (Philipsburg, NJ, USA). Trifluoroacetic acid (TFA) was from Merck Biosciences (Darmstadt, Germany). All the aqueous solutions were prepared using ultra-pure water (18.2 MΩ-cm resistivity at 25°C, total organic carbon (TOC) < 5 ppb).

Sample preparation

Fibrinogens were thawed at 37°C for 5 minutes and equilibrated at room temperature for another 5 minutes before use, filtered with a 0.2 µm ClearLine syringe filter. Concentrations were then determined by absorbance at 280 nm, and adjusted as desired. Thrombin was thawed at 37°C for 1 minute, diluted in HEPES buffer and immediately used.

Fibrin clots were formed by incubating fibrinogen (typically 0.5, 1 and 3 mg/ml) with 0.1 IU/ml thrombin (final concentration) at 37°C during 90 minutes.

Size exclusion chromatography

The molecular distribution of the different fibrinogens was analyzed using a Superose 6 column (GE Healthcare, USA) on an Elite LaChrom system (Hitachi, Japan), coupled with a Dawn Heleos II - Multi-Angle static Light Scattering system (Wyatt Technology, Santa Barbara, USA) and a Optilab T-rex – Refractometer (Wyatt Technology). The same HEPES buffer as before was used. Fifty microliters of fibrinogen (5 mg/ml) were applied and the column was developed at a 0.5 ml/min flow rate. Elution (λ=280 nm), MALLS and Refractometer profiles were analyzed using the ASTRA software from Wyatt Technology.

Dynamic Light Scattering

Dynamic Light Scattering measurements were performed using a CGS-8FS/N069 apparatus from ALV Technology (Manila, Philippines) with a 35 mW, 632.8nm laser from JDSU (Milpitas, CA, USA). Fibrinogens (1 mg/ml) were loaded in 10 mm diameter cylindrical cells, immerged in a toluene bath at 25.0 ± 0.1 °C. Data were collected at 90° for 120 s. Hydrodynamic radii distributions were determined using Contin analysis.

Protein assays

Fibronectin level was assayed on a Siemens BNII nephelometer. Briefly, the sample is mixed with a polyclonal rabbit anti-Human fibronectin to generate immune complexes measured by nephelometry. The fibronectin concentration is deduced by interpolation with a standard curve using the Dade Behring N protein standard PY.

FXIII levels were determined by ELISA using sheep polyclonal anti-Human FXIII (Cedarlane, CL20057A) for the coating and the same polyclonal anti-Human FXIII conjugated with horseradish peroxidase (Cederlane, CL20057HP) as secondary antibodies. Standard human plasma (Siemens, ORKL 17) was used to establish the calibration curve. Results are expressed as International Unit (IU) knowing that 1IU is equivalent to 30 µg/mL.

Reverse phase chromatography coupled to mass spectrometry (MS)

Fibrinogen (100 µg) was vacuum-dried and dissolved in 35 µL of a 8 M urea and 0.4 mM ammonium carbonate solution at pH 8.0. Reduction was done by adding 10 µL of a 40 mM DTT solution in water and incubating the resulting mixture for 20 min at 50°C. After cooling at room temperature, 10 µL of a 80 mM IAM solution in water were added and the solution was incubated at room temperature for 20 min in the dark. Reverse phase high-pressure liquid chromatography (RP-HPLC) was performed using an ACQUITY UPLC system (Waters, Milford,

MA, USA). An amount of 20 µg of sample was injected on a Pursuit 3 diphenyl reverse phase column (150x2.0 mm, 3 µm, Agilent, Santa Clara, CA, USA) equilibrated at 70°C and operated at a flow rate of 200 µL/min. An aqueous solution containing 0.1% TFA and MeCN containing 0.1 % TFA were respectively used as buffer A and buffer B; proteins were eluted by using an increasing gradient of buffer B. After separation, reduced and alkylated fibrinogen chains were detected by UV at 280 nm and MS analysis was achieved by interfacing the UV detector output to a SYNAPT G2-S HDMS mass spectrometer (Waters, Milford, MA, USA) scanning from *m/z* 500 to 2000.

Small angle X-ray Scattering

Small Angle X-ray Scattering (SAXS) experiments were performed at the ID02 line at the European Synchrotron Radiation Facility (ESRF, Grenoble, France). The samples (2 volumes of fibrinogen and 1 of thrombin) were mixed directly in a 12mm x 12mm x 3mm home-made cell with 20 µm mica windows, thermostated at 37± 0.3°C (16). The sample-to-detector distance was set to 7 m and the acquisition time was set to 0.1 s. To avoid radiation-induced degradation of the protein, the cell was displaced by a motorized x-y stage between each measurement in a snake-like fashion, by 2 mm horizontally and 2 mm vertically at the end of a line, i.e. each time by a distance much larger than the beam size (0.5x0.5 mm). The results presented here are the average of the 15 last acquisition times corresponding to steady state scattering curves. The constancy of the signal over several centimeters of the cell shows that the polymerization was finished and that the initial mixing was good. A comparison between two replicate experiments is presented in SI S5, fig. SI.6.

Spectrophotometry

Fibrin gels were formed in 96-well Immulon 2HB plates (Fischer scientific, Illkirch , France) by mixing 2 volumes of fibrinogen (120 µl) and 1 of thrombin (60 µl). Optical density spectra (500 nm to 800 nm) were measured after 90 minutes at 37 ± 0.3 °C using a SpectroStar Omega (BMG Labtech Ortenberg, Germany). For the total volume used in the experiments, the path length was 4.38 mm as determined from calibration using a range of known absorbance.

Optical density data were analyzed using a corrected version of Yeromonahos's (7,15,16) model. A detailed discussion concerning the model choice, pertinence and potential inaccuracies is presented in SI4, with raw data (SI4.1, fig. SI.3) and fit residuals (SI4.3, fig.SI.4, left). It should be kept in mind that the protofibrils numbers, fiber radii and protein densities are not directly measured, but are the result of the fitting of this simple model to the spectral data. Therefore, those data, while quantitative, must be viewed with some caution as the use of a different model may give significantly different results.

Each data point represents the mean and standard deviation calculated from at least 3 individual experiments.

Confocal Microscopy

Microscopic images of fibrin networks were obtained using Alexa488 fluorescent fibrinogen (Invitrogen, Breda, Netherlands) mixed with the unlabelled fibrinogens at a 1:10 ratio. Each mixture was filtered with a 0.2 μm ClearLine syringe filter and the concentrations were then determined by absorbance at 280 nm. Samples were polymerized using 0.1 IU/ml of thrombin and various fibrinogen concentrations (0.5, 1 and 3 mg/ml). Fibrinogen and thrombin were mixed in Eppendorf Tubes 3810X, then rapidly injected in Secure Seal Hybridization Chambers (Grace Biolabs, Bend, OR, USA) and polymerized during 60 minutes at 37° C. Confocal image stacks of the fibrin networks were acquired using a Zeiss LSM710 confocal microscope with a 63x/1.2 water immersion objective (Zeiss, Oberkochen, Germany). The 3D stacks (100 images) were 67.5 μm in the x-y direction and 25 μm in the z direction with resolutions of 100nm and 250nm respectively. The confocal image stacks of the fibrin networks are homogeneous both in the imaging plane and also in depth (data not shown).

For the visualization and presentation of those stacks, we use a recently developed ImageJ plugin: Smooth Manifold Extraction (SME) (17). This method, unlike z-maximum intensity projections, provides a robust 2D representation of 3D objects which preserves local spatial relationship, in particular branching (see SI S6.1, for details and examples).

Finally, the pore size distribution was determined for each frame using the bubble method (18, 19) on each frame and calculated for the complete stack. For details about the segmentation and pore size analysis, see SI S6.2 and SI S6.4.

3 Results.

3.1 Physico-chemical characterization.

Molecular size distribution

The SEC elution profiles of the two fibrinogens are presented in Fig. 1A. They both show a main peak at an elution volume of 11ml, as well as a small broad peak around 9.3 ml, albeit with different intensities (Fib1 > Clottafact). In addition, Fib1 presents a well-defined high molecular weight peak occurring at an elution volume of about 7.5 ml. The analysis of the MALLS and index refraction profiles obtained simultaneously to the elution profile (see material and

methods) yielded the molar masses of the species corresponding to each of those elution peaks as well as their relative concentrations.

A (weight-averaged) molar mass of 325 kDa is obtained for the 11 ml elution peak observed in both fibrinogens, which corresponds closely to the molar mass of fibrinogen monomers (e.g. 13). The ratio of the weight-averaged mass to the number-averaged mass (Mw/Mn) for this peak is below 1.01, indicating good monodispersity. For the broad small peak at 9.5 ml also observed in both fibrinogens, a molar mass of about 1 MDa is obtained, with a significant polydispersity, corresponding probably to a distribution of oligomers. Finally, a mass of about 5 MDa can be assigned to the large peak observed at 7.5 ml in Fib1, corresponding most likely to fibrinogen aggregates. The elution profile and molar masses obtained for Fib1 are in excellent agreement with those of Brookes et al. (13, fig. 3) which were also obtained on Fib1 fibrinogen, but using a size exclusion chromatography column coupled to a small angle X-ray scattering cell.

Those results demonstrate the presence of both oligomers and large aggregates in Fib1 while the Clottafact preparation is close-to- monodisperse with a small amount of oligomers and no detectable aggregates. The relative mass of the aggregates present in Fib1 is found to be of about 4% of the total mass of fibrinogen. In consequence, in the following, Clottafact will be termed as FibWoA for Fibrinogen WithOut Aggregates, while Fib1 will be termed as FibWA for Fibrinogen With Aggregates.

Dispersity analysis by Dynamic Light Scattering

Dynamic Light Scattering (DLS) was used to confirm the above results by determining the average hydrodynamic radius of the different fibrinogens. Since the SEC-MALLS results showed a tri-disperse size distribution, we tried to use a triple exponential fit of the raw correlation spectra to obtain the hydrodynamic size distribution of the molecules. However, those fit were not robust as the result was strongly dependent on the initial values used for the fit. Therefore, we only present the average hydrodynamic radii and the polydispersity indexes obtained by a Contin analysis.

FibWoA fibrinogen has a hydrodynamic radius of 11nm, a hydrodynamic size corresponding well to that of fibrinogen monomers (11,12,20,21). The measured polydispersity index is of 25%, close to the value of 20% below which samples are considered truly monodisperse. Conversely, FibWA fibrinogen has a hydrodynamic radius of 22nm, with a polydispersity index of 52%. This result confirms that FibWA fibrinogen presents mixtures of higher molecular weight species.

RP-HPLC-Mass Spectrometry analysis

The two fibrinogens were further analyzed by RP-HPLC-Mass Spectrometry after reduction and separation of the α, β, and γ chains. MS was used to determine the sequence integrity of the different chains as well as their post-translational modifications. The resulting chromatograms (UV detection) for the two fibrinogen preparations are essentially identical in all respects (see SI2.1, fig. SI.1 and table SI.2 for a description and summary of the MS based identifications). Finally, SDS-PAGE of reduced fibrinogens showed similar γ′/γ chains ratio with 14% for FibWoA and 10% for FibWA (data not shown).

Co-purified proteins content

Co-purified proteins (FXIII and fibronectin) concentrations measured as described in materials and methods are shown in table 1 (see SI2.2, fig. SI.2). The main finding is that FibWoA and FibWA have almost identical composition in co-purified proteins. The only slight difference is the fibronectin content (0.05 vs 0.02 mg/mg) which is low compared to the normal plasmatic value (0.12 mg/mg), and much smaller than the range for which significant structural variations are observed in the literature (0.8 mg/ml) (21, 22) (see SI3, Table SI3).

The results of the physico-chemical analyses are summarized in table 1 and show that the composition of the two fibrinogens is almost identical except for the presence of large molecular weight aggregates.

3.2 Fibrin's ultrastructure

Since polydispersity could influence fibrin structure at the molecular, fiber and network scales, each scale was investigated with the appropriate tool (see figure 1B).

Fibrin fibers internal structure.

We used Small Angle X-Ray Scattering to determine the molecular organization inside fibrin fibers. Figure 2A shows X-ray intensity spectra obtained on mature fibrin clots. The general shape of the scattering curves is identical to those obtained in the literature (7,23). A replicate experiment was performed, yielding an identical spectrum (see SI S5, fig. SI.6), showing the excellent reproducibility of the protocols and methods. Spectra from each fibrin gel showed a main peak at a *q*-vector ~ 0.3 nm^{-1} corresponding to the usual 22.5 nm periodicity of half-staggered fibrin monomers. However, significant differences are observed around this peak, *i.e.* between 0.2 and 0.5 nm^{-1}.

To isolate those differences, we adapted Missori *et al*. (23) method to our data: the log-log scattering curves were first fitted with an order 3 polynomial. This polynomial was then subtracted to the scattering data, yielding the curves shown in figure 2B and 2C. The data were then fitted to two Gaussian distributions (23), one for the main ~22.5nm peak and the other Gaussian for the broad peak (dashed lines).

It is obvious both in figure 2B and in figure 2C that FibWoA fibrin exhibits a much higher amplitude and narrower main peak than FibWA fibrin. FibWoA fibrin also shows a well-defined secondary broad peak that is not observed for FibWA fibrin (Fig. 2C).

FibWoA (Fig. 2B) sharp peak is at q_1 = 0.284 nm^{-1} with a full-width-at-half-maximum (FWHM) of 0.0026 nm^{-1} and the second broader peak is at q_2 = 0.327 nm^{-1} with an FWHM of 0.094 nm^{-1}. The sharp peak can be assigned to a Bragg diffraction from a repeat distance of $d_1=2\pi/q_1=22.2$ nm that corresponds well to the usual periodicity of the half-staggered arrangement of the protofibrils (see fig. 1B). Its FWHM gives a persistence length of 2.4 μm for this longitudinal feature (i.e. along the length of the fiber). This shows that the fibers are straight over this length and without defects in the 22.2 nm half-staggered arrangement. The second, broader peak can be assigned to a repeat distance of $d_2=2\pi/q_2=19.1$ nm which correspond accurately to the lateral dimension of the unit cell of the protofibrils crystal described theoretically by Yang *et al.* (24) and very close to the one observed experimentally by Freyssinet *et al.* (25). This result indicates that the fibers are also close to crystalline laterally (see fig. 1B).

FibWA fibrin (Fig. 2C) shows a small peak at about 0.285 nm^{-1} *i.e.* a longitudinal repeat of 22.1 nm with a FWHM of ~0.01 nm^{-1}, giving a persistence length of ~0.63 μm, about four times smaller than for FibWoA. This indicates that FibWA fibers are less longitudinally organized and/or shorter and/or curvier fibers than FibWoA's. The absence of the large secondary peak observed for FibWoA, shows also a much less organized internal lateral structure.

All those results indicate a major structural change between FibWA and FibWoA at the nanoscale. Indeed, the molecular organization of fibrin fibers made from FibWoA is close to crystalline both longitudinally and laterally while the fibrin fibers made from FibWA are much less organized both longitudinally and laterally.

To extend the scope of the investigation, we performed spectrophotometry measurements (7) for a wider range of experimental conditions and numerous replicates, experiments that would have been unacceptably time-consuming on a synchrotron. Figure 2D shows that fibers from FibWoA clots have about twice as many protofibrils than those from FibWA. This result holds from 0.4 to 3 mg/ml, i.e. up to the normal physiological range. The fitting of the scattering model

to the spectrophotometry data also provides the average radius of the fibers from which the protein density within the fibers can be deduced from $\varrho = \mu/(\pi r^2)$ (e.g. 7). Figure 2E shows that the protein density inside FibWoA fibrin fibers is significantly larger (30-80%) than the density of fibers from FibWA. The range of density values obtained here are in agreement with previous work (15, 26).

To summarize the nanostructural findings, SAXS indicates that FibWoA fibrin fibers are close to crystalline whereas the internal structure of fibers produced from FibWA fibrinogens is significantly less organized, *e.g.* amorphous or fractal as was advocated previously (7, 27, 30). Spectrophotometry results point in the same direction showing that FibWoA fibers possess a significantly higher internal density than FibWA fibers.

Fibrin microstructure: Confocal microscopy

Finally, to check whether the fibrinogen preparation differences could also impact the microstructure, we investigated the network organization of fibrin clots at the micron scale. The 3D microstructure of the different fibrins obtained from confocal 3D stacks is visualized using the "Smooth Manifold Extraction" (SI S6.1, 17). Major differences in the networks geometry are observed (fig.3A).

First, bright spots are observed in FibWA while there are almost none in FibWoA (red arrows in insets of fig.3A, right). Second, differences in fibers geometry are also observed. FibWoA fibrin shows needle-like fibers that are always perfectly straight over several μm, while FibWA produces networks with shorter and some curved fibers (highlighted by the white arrows in FibWA inset). The observed straightness of FibWoA fibers is in perfect agreement with the large persistence length obtained in the SAXS measurements while FibWA fibers relative shortness or curviness is also in agreement with the lower persistence length obtained from the SAXS measurements.

Finally, FibWoA's fibrin shows usually a rather small number of branches per branching node, typically looking like the contact point between needle-like fibers while FibWA shows star-like patterns, with several asymmetrical branches per node.

4 Discussion

The first aim of this article is to assess whether or not fibrinogen dispersity influences the ensuing fibrin ultrastructure and how important it is with respect to compositionally-induced changes. A possibility to obtain such products would have been to replicate the fractionation process proposed by Huang et al (11), followed by a complete determination of the

fractionated fibrinogen composition. However, this fibrinogen fractionation method has been shown at least once to produce significant amounts of in-column degradation products (13) which contaminated the elution peaks of the undegraded material. Besides, such a method allows obtaining only very low fibrinogen concentrations (below 1g/L). This forbids any study in the physiological range. In consequence, we chose to test existing commercial fibrinogens preparations for dispersity. Among those we tested, only FibWoA (Clottafact) showed a close-to-monodisperse profile. For the second, polydisperse fibrinogen, we chose FibWA (Fib1) fibrinogen which is the *de facto* reference since it has been used in the large majority of works dealing with purified fibrin structure and rheology (see SI1).

In the first part of this work we determined the FibWA and FibWoA compositions by measuring their FXIII, fibronectin, α, β and γ intact-chains content, γ/γ' ratio as well as their N-glycosylation and post-translational modifications (see table 1). To evaluate if the variations in composition observed between FibWA and FibWoA may have a significant impact on fibrin structure, we compiled the compositional effects on fibrin structure observed in the literature. This compilation (table S3.1 in SI3) shows that the measured FibWoA-FibWA compositional differences are (very) small compared to the compositional range of variation necessary to obtain measurable structural changes in fibrin structure. So, the slight compositional variance between FibWoA and FibWA cannot explain the large structural differences observed between FibWoA and FibWA fibrins. In consequence, those structural differences can only be the consequence of the significant quantity (4% in mass) of large aggregates found in FibWA since FibWoA does not possess such aggregates. Surprisingly, aggregates-induced structural differences are as large as or larger than those induced by compositional changes under constant reaction conditions, as shown in SI3 table SI3.1. Therefore, the presence of aggregates is a major determinant of fibrin polymerization and structure and its effect persists at all concentrations used in this work, from 0.5 mg/mL to 3 mg/mL.

Those aggregates correspond probably to the bright spots observed in the FibWA images only. Furthermore, since aggregates are known to accelerate the initial growth of the fibres (12), their main role should be to nucleate new fibres independently of the normal fibre formation mechanism. In consequence, the larger the aggregates content is, the more fibres should be nucleated. Since the total fibrinogen mass is conserved, it further derives that the larger the aggregates content is, the smaller the average number of protofibrils per fibre should be in the ensuing fibrin.

Since the FibWoA and FibWA have practically identical compositions, this hypothesis can be checked by mixing increasing quantities of FibWA with FibWoA, experiment which amounts

to increasing the aggregates content. Fig. 3B shows a large (~100%) linear decrease in the number of protofibrils per fiber as a function of the aggregate (~FibWA) content, as expected from the simple argument presented above. Confocal images of the same mixtures (SI.6.3 fig. SI.10) show also a progressive change from straight fibers without bright spots to shorter, curvier fibers linking bright aggregates, supporting the above explanation. Fig 3B further shows that the internal density of the fibers is significantly modified by the presence of aggregates, albeit in a less dramatic fashion than the number of protofibrils.

As deduced from the confocal images above, a plausible hypothesis is that a significant part of the FibWA fibers actually grow from activated fibrinogen present in the aggregates, hindering the lateral growth through several phenomena. First, there will be steric hindrance because of the local presence of the aggregate and of the several neighboring fibers as shown in fig 4A. Second, to link between aggregates, the fibers can stick upon each other or the fiber can bend. In the latter case, such a bending will discourage lateral growth because the 22.5 nm periodicity will be partly lost. Finally, recent results suggest that it is the twisted conformation of both fibrinogen monomers and protofibrils that promotes the assembly of protofibrils into fibres (12), in agreement with observations by Weisel's group (29). Consequently, aggregates could disrupt the initial fibres natural helical geometry (12), forbidding a proper local lateral aggregation, generating defects or holes in the structure of the fibres. All of these possible mechanisms lead to the same result: a net decrease in the internal density of the fibres. This interpretation also explains the absence of well-defined lateral structure in FibWA fibres as observed in the SAXS experiments. Conversely, in the absence of aggregates, ideal needle-like fibres can grow and then stick together when they meet. So, once again, the larger the aggregates content is, the larger the number of perturbed, low density fibres will be, giving an average decrease in fibre density as observed in fig. 3B.

The main limitation of the present work lies in the use of the simple model proposed by Yeromonahos et al. to analyse the turbidity data [6]. Recently, a complex turbidity model was proposed by Ferri et al to analyse similar data [26], model based on the hypothesis that fibrin gels are properly described by fractal networks. This model shows that variations in the fractal dimension and, to a lesser extent, pore size of filamentous gels can strongly affect the determination of the fibres parameters derived from turbidity data [26]. If large differences in fractal dimension were determined between the fibrin gels produced in our work, it would undermine significantly the proposed mechanism of influence of the aggregates on the fibrin gels ultrastructure.

However, we doubt that those fibrin gels can be properly represented by fractal networks since no scale-recursivity is observed on the confocal images. Furthermore, the use of Ferri's model requires measuring reliably the 3D fractal dimension from confocal microscopy data. Unfortunately, very large differences in methods and results between authors can be found in the literature (see SI S4.2). For those reasons, we chose to use the much simpler Yeromonahos model, which consistency is favourably checked against pore size measurements while supposing that the fractal dimension of the network is 1 (see SI S7.3 and fig. S12 for details). This important issue of the fractality of filamentous gels and the potential need for a fractal model to analyse turbidity data will be the subject of a forthcoming article.

Conclusions

We have first shown that Clottafact's fibrinogen is composed almost exclusively of fibrinogen monomers whereas Fib1 possess a significant amount of large aggregates. Conversely, the detailed physico-chemical analyses of Clottafact and Fib1 show that their compositions are sufficiently similar not to influence the structure of the ensuing fibrins. Small angle X-ray scattering demonstrates that the internal structure of Clottafact's (FibWoA) fibrin fibers is close to crystalline both laterally and longitudinally with a longitudinal persistence length of several microns. Conversely, SAXS shows that Fib1 (FibWA) fibers are much more disorganized with no perceptible lateral organization and a longitudinal persistence length of a few hundreds of nanometers. Those nano-structural observations are confirmed at the microscale by direct confocal imaging. Clottafact fibrin displays long, needle-like fibers while Fib1 fibrin shows short and curved fibers in agreement with the SAXS persistence length measurements. Those results are further strengthened by spectrophotometry measurements which confirm the significantly larger density of the Clottafact fibers with respect to Fib1 ones. Those structural differences hold at all studied concentrations including physiological ones and demonstrate that the size dispersity of fibrinogen in purified systems is one of the main parameters determining fibrin fibers ultrastructure, parameter that has been mostly overlooked. Indeed, the effect of modifying the dispersity is surprisingly large, larger than changing any other aspect of the fibrinogen preparation.

Those results open outstanding questions regarding the precise mechanisms by which the presence of aggregates can influence to such an extent the polymerization of fibrin and, therefore, concerning fibrin polymerization itself. Furthermore, given the extensive structural modifications accompanying the presence of aggregates, the mechanical properties of fibrin clots formed from monodisperse fibrinogens may be very significantly different from the

polydisperse ones and could be of paramount interest in tissue engineering on fibrin scaffolds as well as for the design of fibrin glues.

Finally, the actual amount of aggregates in circulating fibrinogen is not known as only a few studies investigated the multiscale structure of fibrin formed in plasma. Such investigations could be of outstanding interest in hemostasis, in particular in relation to thrombosis related diseases.

Authors' contributions

XG, LS and FC conducted and analyzed the experiments in small angle X-ray scattering, multi-wavelength spectrophotometry, dynamic light scattering, confocal microscopy and gel filtration chromatography. GC and NB conducted and analyzed the experiments in reverse phase chromatography, mass spectrometry and ELISA dosages. FC, BP and ZT conceived and directed the research. XG, BP and FC wrote the manuscript. All authors contributed to the final version of the manuscript.

Conflict of interest

XG, LS, BP, and FC declare no conflict of interest. ZT, GC, and NB are employees of the Laboratoire Français du Fractionnement et des Biotechnologies.

Acknowledgment

The authors gratefully acknowledge the help of Marie-Claire Dagher and Caroline Mas for gel-filtration experiments, Christophe Travelet for DLS experiments, Denis Roux, Emmanuelle Bigo and Michael Sztucki (local contact) for the SAXS experiments performed on beamline ID02 (ESRF, Grenoble, France). The SEC-MALLS-RI was performed at the Grenoble Instruct-ERIC Center within the Grenoble Partnership for Structural Biology. Imaging was performed on the confocal microscope of the Cell and Tissue Imaging facility (IBiSA, TIMC-IMAG laboratory, Grenoble).

The authors are also grateful to Marguerite Rinaudo for enlightening discussions and Marie-Hélène André for a careful reading of the manuscript.

Xabel García was funded by the LabEx Tec 21 (Investissements d'Avenir - grant agreement n°ANR-11-LABX-0030).

References

1. Undas, A., and R. A. Ariens. 2011. Fibrin clot structure and function: a role in the pathophysiology of arterial and venous thromboembolic diseases. Arteriosclerosis, Thrombosis, and Vascular Biology 31:e88-99.

2. Ariens, R. A. 2013. Fibrin(ogen) and thrombotic disease. J Thromb Haemost 11 Suppl 1:294-305.

3. Longstaff, C., and K. Kolev. 2015. Basic mechanisms and regulation of fibrinolysis. J Thromb Haemost 13 Suppl 1:S98-105.

4. Ferry, J. D. 1952. The Mechanism of Polymerization of Fibrinogen. Proc Natl Acad Sci U S A 38:566-569.

5. Di Stasio, E., Nagaswami , C., Weisel, J.W., Di Cera E. 1998. Cl^- Regulates the Structure of the Fibrin Clot. Biophys. J. 75: 1973–1979

6. Yeromonahos, C., R. Marlu, B. Polack, and F. Caton. 2012. Antithrombin-independent effects of heparins on fibrin clot nanostructure. Arterioscler Thromb Vasc Biol 32:1320-1324.

7. Yeromonahos, C., B. Polack, and F. Caton. 2010. Nanostructure of the Fibrin Clot. Biophys J 99:2018-2027.

8. Domingues, M. M., Macrae, F. L., Duval, C., McPherson, H. R., Bridge, K. I., Ajjan, R. A., ... & Ariëns, R. A. (2016). Thrombin and fibrinogen γ′ impact clot structure by marked effects on intrafibrillar structure and protofibril packing. *Blood*, 127(4), 487-495.

9. Kurniawan, N. A., van Kempen, T. H., Sonneveld, S., Rosalina, T. T., Vos, B. E., Jansen, K. A., ... & Koenderink, G. H. (2017). Buffers strongly modulate fibrin self-assembly into fibrous networks. *Langmuir* 33 (25): 6342–6352

10. Ping, L., Huang, L., Cardinali, B., Profumo, A., Gorkun, O. V., & Lord, S. T. (2011). Substitution of the human αC region with the analogous chicken domain generates a fibrinogen with severely impaired lateral aggregation: fibrin monomers assemble into protofibrils but protofibrils do not assemble into fibers. *Biochemistry*, 50(42), 9066-9075.

11. Huang, L., and S. T. Lord. 2013. The isolation of fibrinogen monomer dramatically influences fibrin polymerization. *Thromb Res* 131:e258-263.

12. Huang, L., J. P. Hsiao, C. Powierza, R. M. Taylor, 2nd, and S. T. Lord. 2014. Does topology drive fiber polymerization? Biochemistry 53:7824-7834.

13. Brookes, E., Pérez, J., Cardinali, B., Profumo, A., Vachette, P., & Rocco, M. (2013). Fibrinogen species as resolved by HPLC-SAXS data processing within the UltraScan Solution Modeler (US-SOMO) enhanced SAS module. *Journal of applied crystallography*, *46*(6), 1823-1833

14. Trinkle, S., & Friedrich, C. (2001). Van Gurp-Palmen-plot: a way to characterize polydispersity of linear polymers. *Rheologica Acta*, 40(4), 322-328.13.

15. Carr, M. E., Jr., and J. Hermans. 1978. Size and density of fibrin fibers from turbidity. Macromolecules 11:46-50.

16. Yeromonahos, C. (2011). Nanostructure des fibres de fibrine (PhD dissertation). Université Joseph Fourier, Grenoble, France.

17. Shihavuddin, A., Basu, S., Rexhepaj, E., Delestro, F., Menezes, N., Sigoillot, S. M., ... & Genovesio, A. (2017). Smooth 2D manifold extraction from 3D image stack. *Nature Communications*, *8*, 1555

18. Molteni, M., Magatti, D., Cardinali, B., Rocco, M., & Ferri, F. (2013). Fast two-dimensional bubble analysis of biopolymer filamentous networks pore size from confocal microscopy thin data stacks. Biophysical journal, 104(5), 1160-1169.

19. Münster, S., & Fabry, B. (2013). A simplified implementation of the bubble analysis of biopolymer network pores. Biophysical journal, 104(12), 2774-2775

20. Cardinali, B., A. Profumo, A. Aprile, O. Byron, G. Morris, S. E. Harding, W. F. Stafford, and M. Rocco. 2010. Hydrodynamic and mass spectrometry analysis of nearly-intact human fibrinogen, chicken fibrinogen, and of a substantially monodisperse human fibrinogen fragment X. Arch Biochem Biophys 493:157-168.

21. Carr, M. E., Gabriel, D. A., & McDonagh, J. (1987). Influence of factor XIII and fibronectin on fiber size and density in thrombin-induced fibrin gels. Translational Research, 110(6), 747-752.

22. Ramanathan, A., & Karuri, N. (2014). Fibronectin alters the rate of formation and structure of the fibrin matrix. Biochemical and biophysical research communications, 443(2), 395-399.

23. Missori, M., M. Papi, G. Maulucci, G. Arcovito, G. Boumis, A. Bellelli, G. Amiconi, and M. De Spirito. 2010. Cl− and F− anions regulate the architecture of protofibrils in fibrin gel. European Biophysics Journal 39:1001-1006.

24. Yang, Z., I. Mochalkin, and R. F. Doolittle. 2000. A model of fibrin formation based on crystal structures of fibrinogen and fibrin fragments complexed with synthetic peptides. Proc Natl Acad Sci U S A 97:14156-14161.

25. Freyssinet, J. M., J. Torbet, G. Hudry-Clergeon, and G. Maret. 1983. Fibrinogen and Fibrin Structure and Fibrin Formation Measured by Using Magnetic Orientation. Proc Natl Acad Sci U S A 80:1616-1620.

26. Ferri, F., Calegari, G. R., Molteni, M., Cardinali, B., Magatti, D., & Rocco, M. (2015). Size and Density of Fibers in Fibrin and Other Filamentous Networks from Turbidimetry: Beyond a Revisited Carr–Hermans Method, Accounting for Fractality and Porosity. *Macromolecules*, *48*(15), 5423-5432.

27. Guthold, M., Liu, W., Stephens, B., Lord, S. T., Hantgan, R. R., Erie, D. A., ... & Superfine, R. (2004). Visualization and mechanical manipulations of individual fibrin fibers suggest that fiber cross section has fractal dimension 1.3. *Biophysical Journal*, 87(6), 4226-423615.

28. Lang, N. R., Münster, S., Metzner, C., Krauss, P., Schürmann, S., Lange, J., ... & Fabry, B. (2013). Estimating the 3D pore size distribution of biopolymer networks from directionally biased data. *Biophysical journal*, *105*(9), 1967-1975.

29. Weisel, J. W., & Nagaswami, C. (1992). Computer modeling of fibrin polymerization kinetics correlated with electron microscope and turbidity observations: clot structure and assembly are kinetically controlled. *Biophysical journal*, 63(1), 111-128.

30. Li, W., Sigley, J., Baker, S. R., Helms, C. C., Kinney, M. T., Pieters, M., ... & Guthold, M. (2017). Nonuniform Internal Structure of Fibrin Fibers: Protein Density and Bond Density Strongly Decrease with Increasing Diameter. *BioMed research international*, vol. 2017, Article ID 6385628.

Table 1: Physico-chemical characteristics of the two fibrinogens.

	FibWoA	FibWA
Presence of aggregates	Not detectable	4% in total Fg mass
Average hydrodynamic radius (nm)	11	22
FXIII (U/mg Fg)	0.26	0.25
Fibronectin (mg/mg Fg)	0.05	0.02
Post-translational modifications	identical	Identical
Intact α-chains (% vs FibWoA)	100%	95%
Respective intact β and γ chains	100%	100%
γ′/γ chains ratio (%)	14	10

Figures legends:

Figure 1. A: Molecular size distribution of Clottafact and Fib1 determined by size exclusion chromatography. B. Multiscale structure of the fibrin clot.

Figure 2. A: Scattered intensity of small angle X-ray for fibrin clots (1mg/ml). B and C : Relative intensity of around the 22.5nm periodicity peak for resp. FibWoA and WibWA. Continuous lines are the total fit, while dashed lines are the individual peaks. The R^2 values are the goodness-of-fit coefficients. **D: Final number of protofibrils and E: final protein density inside fibrin fibers.** Inset: fibers radii vs fibrinogen concentration.

Figure 3. A: Qualitative geometry of the fibrin networks. Smooth Manifolds were extracted from 3D confocal microscopy stacks at [Fg]=3mg/mL. White arrows show curved fibers, while red arrows show bright dots. Frames are 67.5 μm wide. The insets are x2 enlargements of a portion of the original SME image (12x12 μm**). B: Number of protofibrils, protein density and radius (inset) vs content in FibWA.** Closed circles: Protofibrils number; open circles: Protein density; Inset: fibers average radius.

Figure 4. Proposed fibrin formation mechanism A: in the presence of aggregates (FibWA). B: in the absence of aggregates (FibWoA).

A

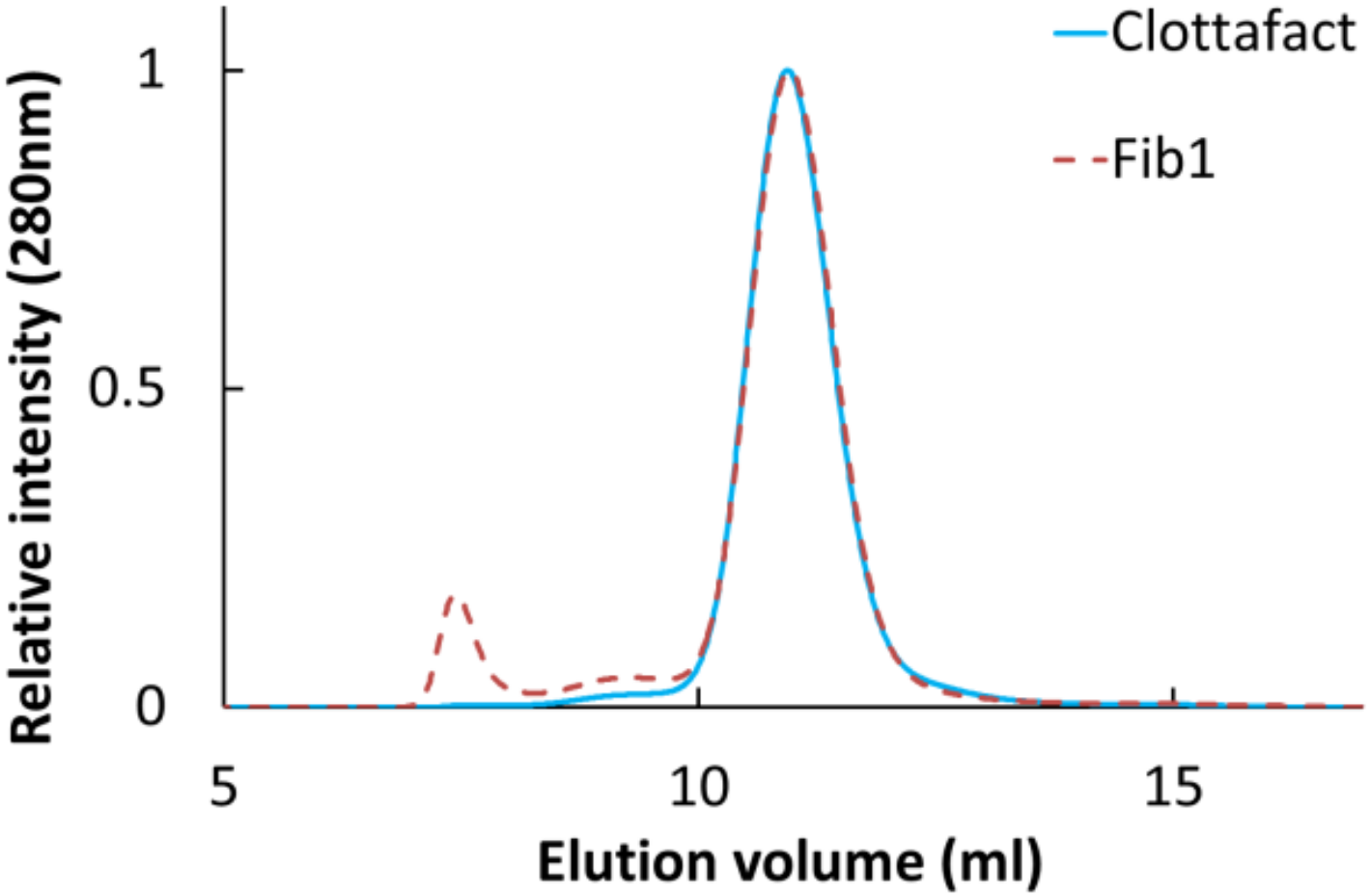
Clottafact
Fib1
Relative intensity (280nm)
1
0.5
0
5
10
15
Elution volume (ml)

B

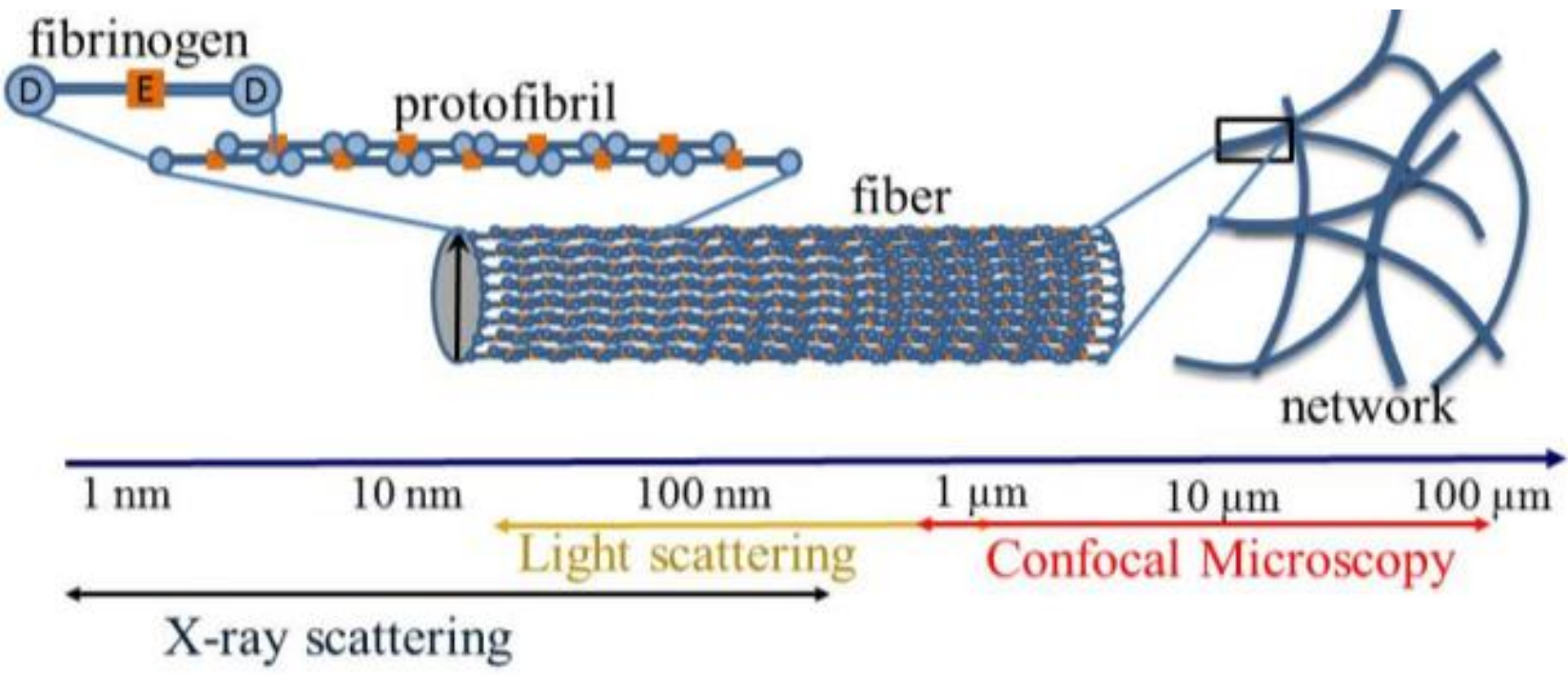
fibrinogen
D
E
D
protofibril
fiber
network
1 nm
10 nm
100 nm
1 µm
10 µm
100 µm
Light scattering
Confocal Microscopy
X-ray scattering

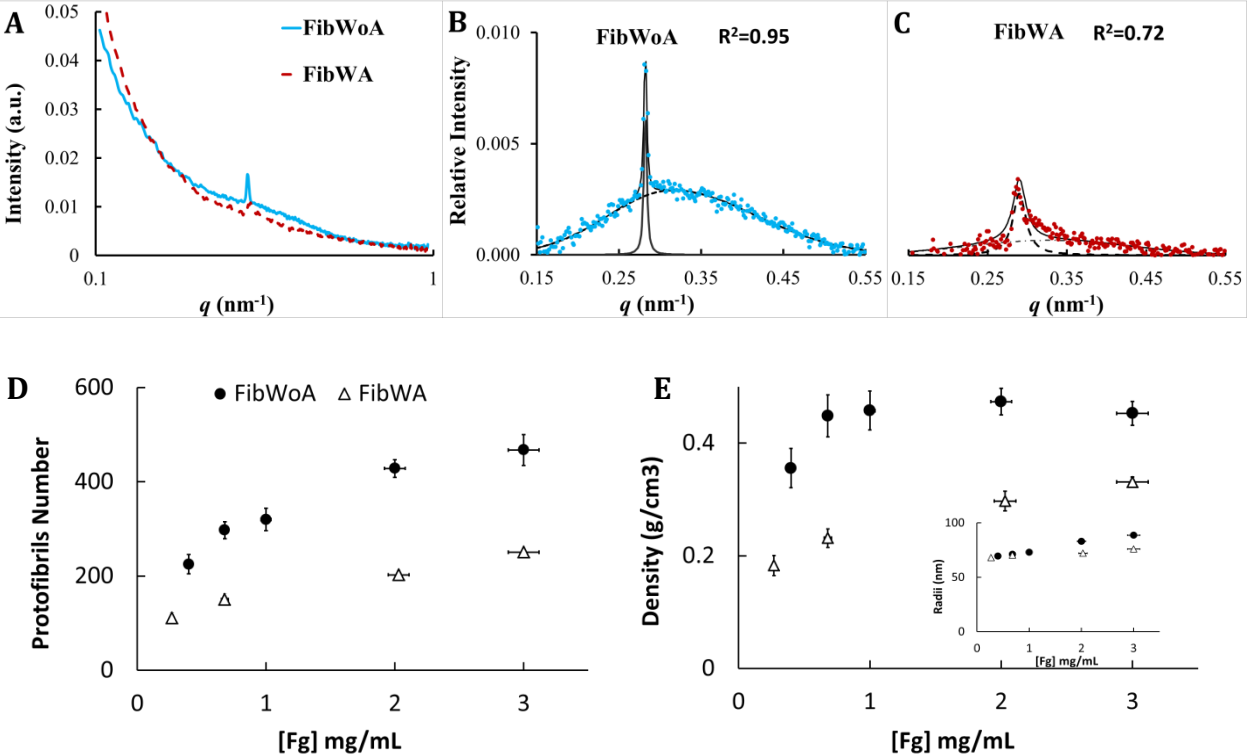
A
FibWoA
FibWA
Intensity (a.u.)
0.05
0.04
0.03
0.02
0.01
0
0.1
1
q (nm-1)
B
FibWoA
R2=0.95
Relative Intensity
0.010
0.005
0.000
0.15
0.25
0.35
0.45
0.55
q (nm-1)
C
FibWA
R2=0.72
0.15
0.25
0.35
0.45
0.55
q (nm-1)
D
FibWoA
FibWA
Protofibrils Number
600
400
200
0
0
1
2
3
[Fg] mg/mL
E
Density (g/cm3)
0.4
0.2
0
0
1
2
3
[Fg] mg/mL
Radii (nm)
100
50
0
0
1
2
3
[Fg] mg/mL

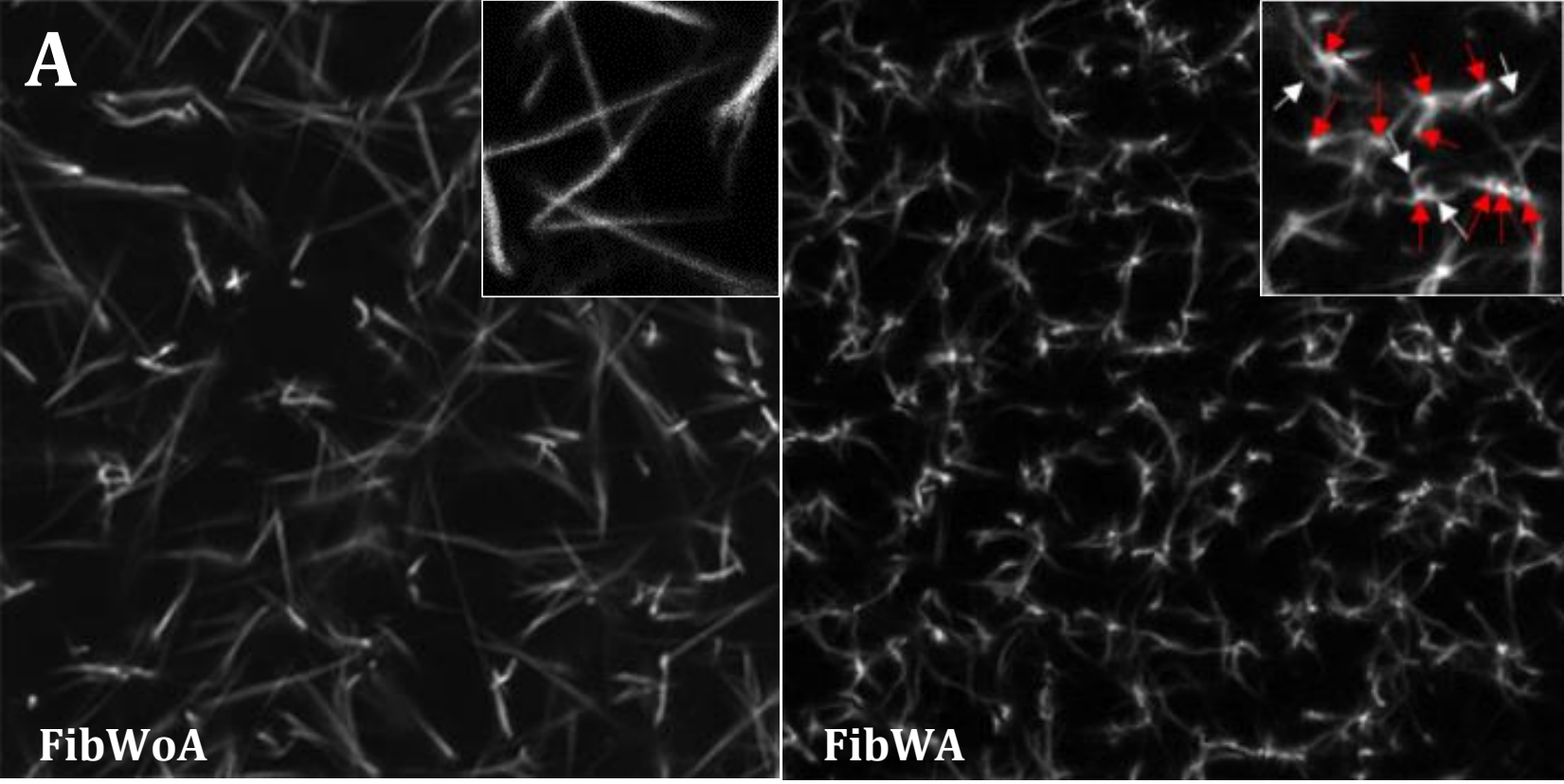
A
FibWoA
FibWA

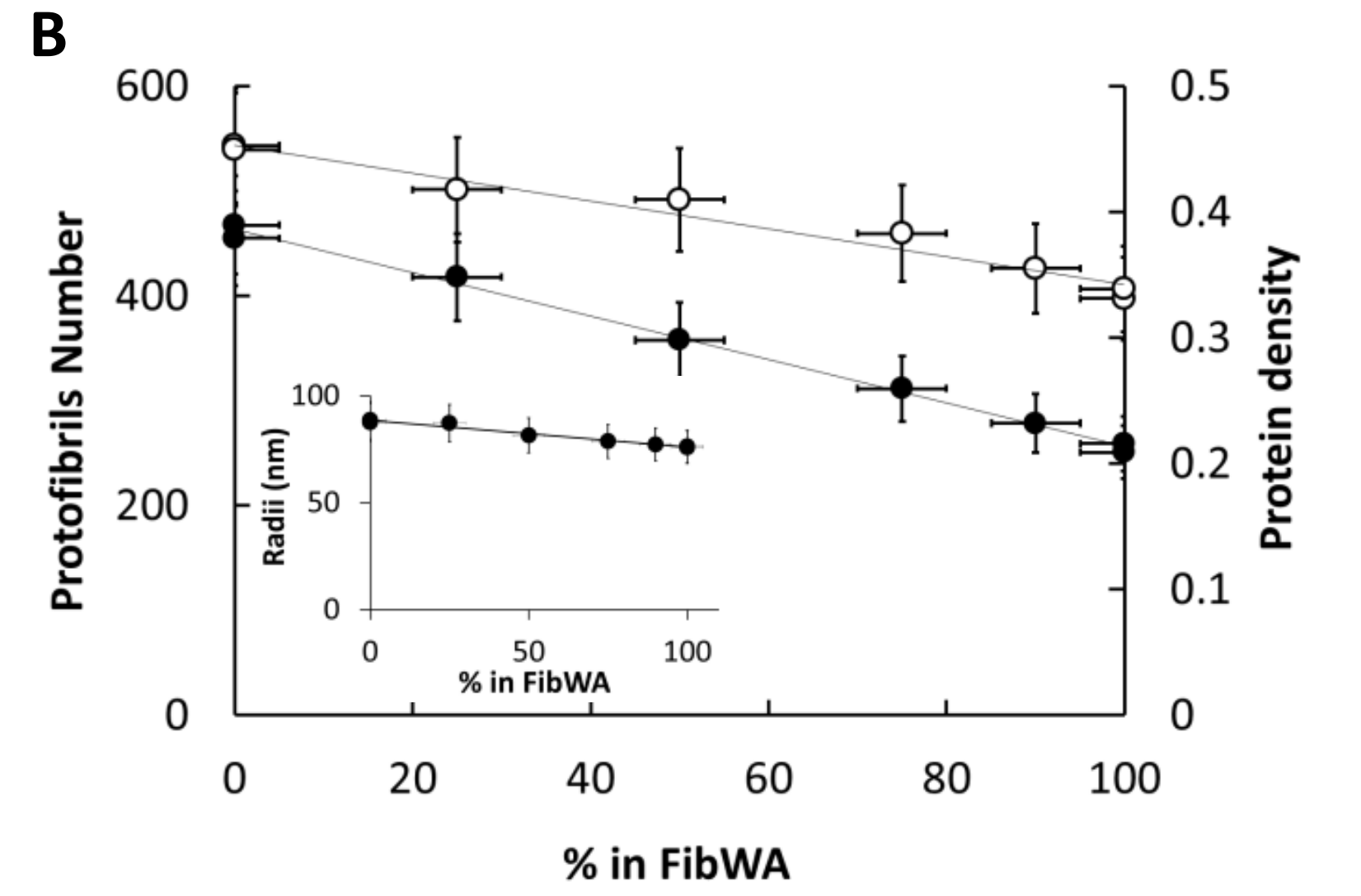
B
600
400
200
0
Protofibrils Number
0.5
0.4
0.3
0.2
0.1
0
Protein density
0
20
40
60
80
100
% in FibWA
100
50
0
Radii (nm)
0
50
100
% in FibWA

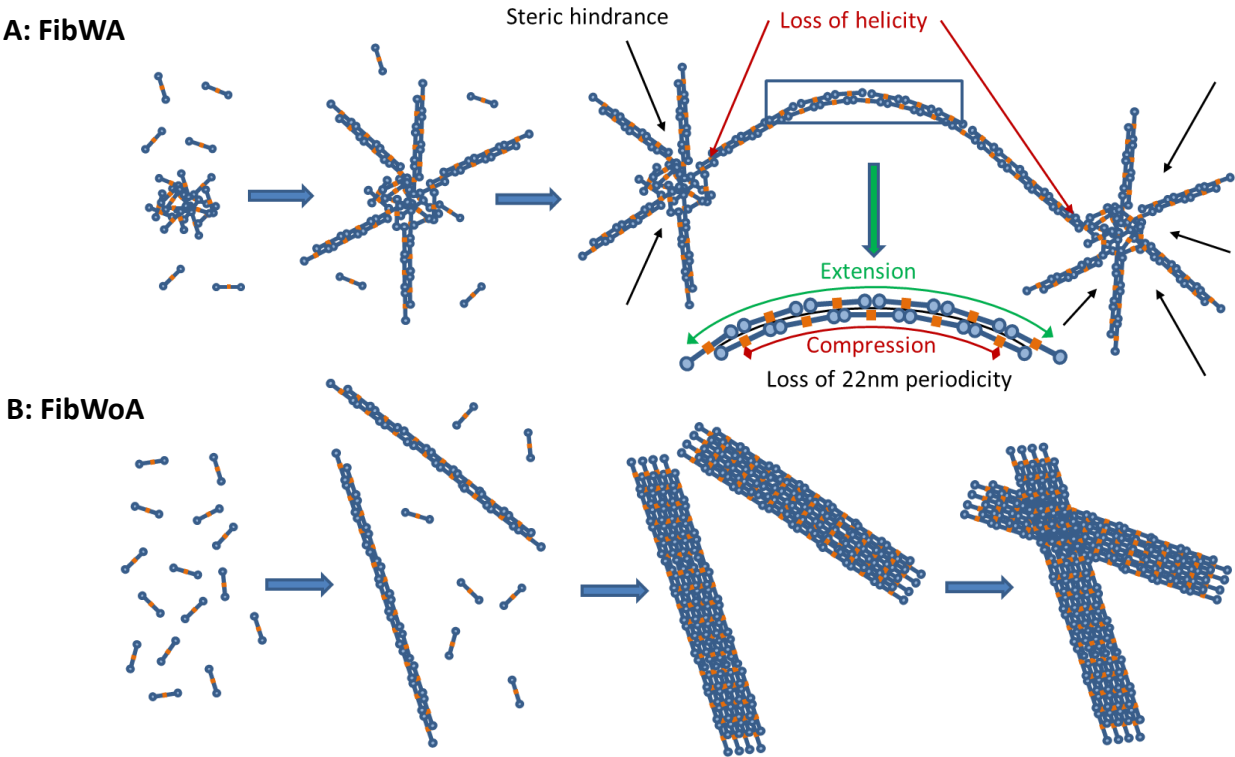
A: FibWA
Steric hindrance
Loss of helicity
Extension
Compression
Loss of 22nm periodicity
B: FibWoA